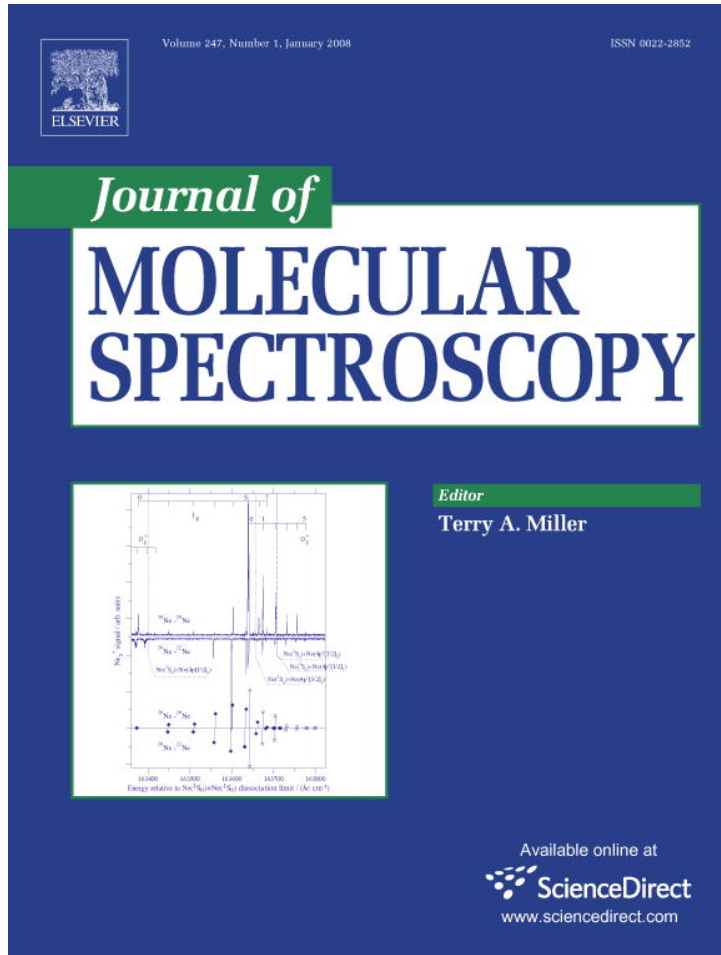


Provided for non-commercial research and education use.
Not for reproduction, distribution or commercial use.



This article was published in an Elsevier journal. The attached copy
is furnished to the author for non-commercial research and
education use, including for instruction at the author's institution,
sharing with colleagues and providing to institution administration.

Other uses, including reproduction and distribution, or selling or
licensing copies, or posting to personal, institutional or third party
websites are prohibited.

In most cases authors are permitted to post their version of the
article (e.g. in Word or Tex form) to their personal website or
institutional repository. Authors requiring further information
regarding Elsevier's archiving and manuscript policies are
encouraged to visit:

<http://www.elsevier.com/copyright>



Fourier transform spectroscopy of $^{12}\text{C}^{18}\text{O}_2$ and $^{16}\text{O}^{12}\text{C}^{18}\text{O}$ in the 3800–8500 cm^{-1} region and the global modeling of the absorption spectrum of $^{12}\text{C}^{18}\text{O}_2$

L. Wang ^a, V.I. Perevalov ^b, S.A. Tashkun ^b, K.-F. Song ^a, S.-M. Hu ^{a,*}

^a Hefei National Laboratory for Physical Sciences at Microscale, Department of Chemical Physics,
University of Science and Technology of China, Hefei 230026, China

^b Laboratory of Theoretical Spectroscopy, Institute of Atmospheric Optics, Siberian Branch, Russian Academy of Sciences,
1, Akademicheskii av., 634055 Tomsk, Russia

Received 21 May 2007; in revised form 26 September 2007

Available online 16 October 2007

Abstract

The absorption spectrum of the ^{18}O enriched carbon dioxide has been recorded at Doppler limited resolution with a Fourier transform spectrometer in the spectral range 3800–8500 cm^{-1} . Seventeen cold bands ($14\Sigma-\Sigma$ and $3\Sigma-\Pi$) and nine hot bands ($9\Pi-\Pi$) of $^{12}\text{C}^{18}\text{O}_2$, nineteen cold bands ($18\Sigma-\Sigma$ and $1\Sigma-\Pi$) and eighteen hot bands ($6\Sigma-\Sigma$, $9\Pi-\Pi$ and $3\Delta-\Delta$) of $^{16}\text{O}^{12}\text{C}^{18}\text{O}$ have been observed. Among them, 14 $^{12}\text{C}^{18}\text{O}_2$ bands and 12 $^{16}\text{O}^{12}\text{C}^{18}\text{O}$ bands are observed for the first time. The spectroscopic parameters G_v , B_v , and centrifugal distortion constants, have been determined for all observed bands. Effective Hamiltonian parameters for the $^{12}\text{C}^{18}\text{O}_2$ isotopic species are retrieved from the global fitting of the observed line positions presented in this paper and collected from the literature. As the result, 65 obtained effective Hamiltonian parameters reproduce 5443 observed line positions of 73 $^{12}\text{C}^{18}\text{O}_2$ bands with RMS = 0.00145 cm^{-1} .

© 2007 Elsevier Inc. All rights reserved.

Keywords: Carbon dioxide; Infrared; Fourier transform spectroscopy; Line positions; Global modeling

1. Introduction

The infrared absorption spectroscopy of carbon dioxide is of great interest for many important applications. This paper is one of the series of our publications devoted to the global modeling of high resolution spectra of carbon dioxide molecule [1–17]. In this paper we are concentrated on two ^{18}O consisted isotopologues: $^{16}\text{O}^{12}\text{C}^{18}\text{O}$ and $^{12}\text{C}^{18}\text{O}_2$ (natural abundance 0.0039471 and 0.0000039573, respectively). We have undertaken a systematic measurement of line positions of these isotopic species using Fourier Transform Spectrometer in Hefei. These isotopologues could have important contribution to the absorp-

tion by very dense Venus atmosphere which is dominated by CO_2 . When this work started there were no publications concerning the measurements of high resolution spectra of $^{12}\text{C}^{18}\text{O}_2$ in the region above 4000 cm^{-1} , except the band 20013–00001 centered at 4721.92 cm^{-1} which was detected in Venus spectra [18]. In parallel to our study, Toth et al. [19] reported the strong bands of $^{16}\text{O}^{12}\text{C}^{18}\text{O}$ and $^{12}\text{C}^{18}\text{O}_2$ in this region. The ro-vibrational transitions of $^{16}\text{O}^{12}\text{C}^{18}\text{O}$ in the region 3600–8500 cm^{-1} have been reported in Refs. [13,18–21]. The present work provides a comparison with the available data of $^{16}\text{O}^{12}\text{C}^{18}\text{O}$ and $^{12}\text{C}^{18}\text{O}_2$ and also fills some gaps in this region.

This paper is organized as following: Section 2 presents the experimental details, Section 3 gives the rotational analysis and vibrational assignments, Section 4 deals with the global fit of the effective Hamiltonian parameters of $^{12}\text{C}^{18}\text{O}_2$ and the conclusions are given in Section 5.

* Corresponding author. Fax: +86 551 360 2969.
E-mail address: smhu@ustc.edu.cn (S.-M. Hu).

2. Experimental details

The ^{18}O enriched carbon dioxide sample was purchased from Icon Services. The stated isotopic concentration for the oxygen atom is 84.3% of ^{18}O . The isotope abundance was studied by a photo-ionization mass spectroscopy (PIMS) experiment. PIMS was measured with an electron time-of-flight mass spectrometer in the photochemistry end-station of National Synchrotron Radiation Laboratory, Hefei. The abundances of $^{12}\text{C}^{18}\text{O}_2$ and $^{16}\text{O}^{12}\text{C}^{18}\text{O}$ were determined as 63.8% and 28.4%, respectively. The accuracy of the PIMS measurement was estimated to be about 0.1%.

The absorption spectra were recorded in the spectral range from 4000 to 9500 cm^{-1} , with a Bruker IFS 120HR Fourier-transform spectrometer (FTS) equipped with a path length adjustable multi-pass gas cell. The maximum optical path length is 105 m. A tungsten source, CaF_2 beam splitter were used in all experiments. The cell was operated at room temperature, stabilized by an air-conditioning system. The pressure was measured using two capacitance manometers of 200 Pa and 133 hPa full-scale ranges with an overall accuracy of 0.5%. Different band-pass optical filters were applied to improve the signal to noise ratio. For accurate line position measurements, no apodization function was applied. The line positions were calibrated using the absorption lines of water (present as an impurity in the cell) given in HITRAN database [22]. The experimental conditions are presented in Table 1. The accuracy of the unblended lines recorded with a good signal to noise ratio was estimated to be better than 0.001 cm^{-1} . Altogether more than 4700 scans were co-added to improve the signal-noise-ratio. An overview and a small portion of the recorded spectrum are presented in Figs. 1 and 2, respectively.

3. Rotational analysis and vibrational assignment

The band by band rotational analysis was performed using the standard expression for the rotational energy levels in a given vibrational state:

$$\begin{aligned} E_v(J, \ell_2) = & G_v + B_v [J(J+1) - \ell_2^2] \\ & - D_v [J(J+1) - \ell_2^2]^2 \\ & + H_v [J(J+1) - \ell_2^2]^3. \end{aligned} \quad (1)$$

Table 1
Experimental conditions

Spectral region (cm^{-1})	Pressure (Pa)	Path length (m)	Resolution (cm^{-1})	Detector	Sample scans
3500–7500	3476	105	0.015	InSb	4752
3500–7500	3223	15	0.015	InSb	1386
3500–7500	531	15	0.01	InSb	938
5000–9000	3348	105	0.017	Ge	4928
5000–9000	3246	15	0.017	Ge	1792

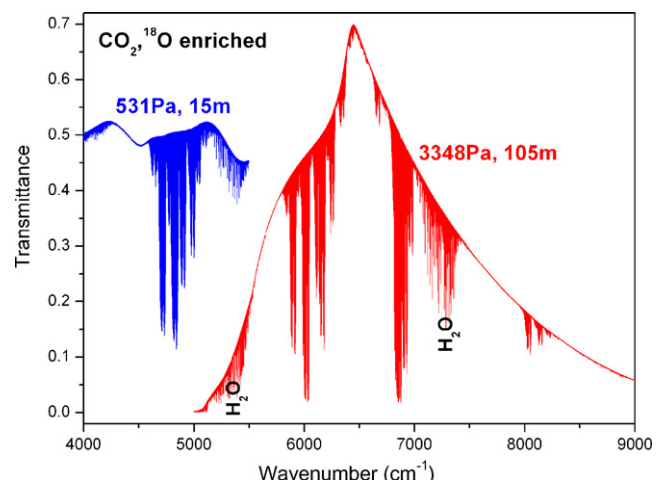


Fig. 1. An overview of the Fourier-transform absorption spectrum of $\text{O}-18$ enriched CO_2 in the region $4000\text{--}9000 \text{ cm}^{-1}$.

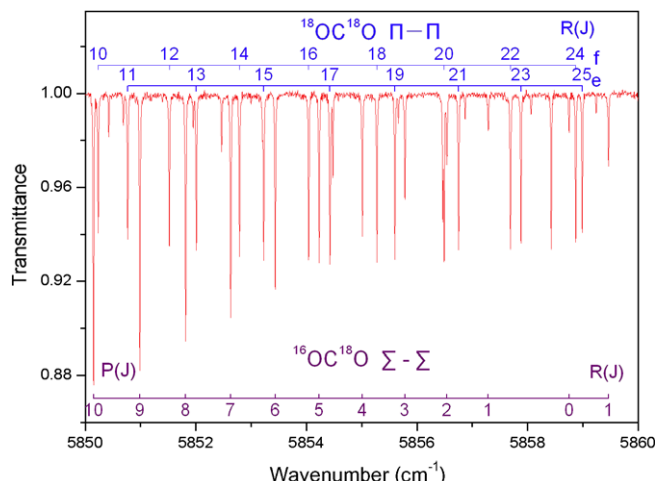


Fig. 2. A small portion of the Fourier-transform absorption spectrum in the region $5850\text{--}5860 \text{ cm}^{-1}$. The P-branch of the $\Sigma-\Sigma$ cold band centered at 5858.02 cm^{-1} of $^{16}\text{O}^{12}\text{C}^{18}\text{O}$ and the R-branch of the $^{12}\text{C}^{18}\text{O}_2 \Pi-\Pi$ hot band centered at 5842.86 cm^{-1} are shown. Experimental conditions: O-18 enriched CO_2 sample, total sample pressure: 3348 Pa, absorption path length: 105 m.

Here G_v is the vibrational term value, B_v is the rotational constant, D_v is centrifugal distortion constants, ℓ_2 is the quantum number associated to the vibrational angular momentum. These constants for an upper state have been fitted to the observed line positions of the respective observed band. The lower state constants (for the ground

Table 2
Spectroscopic constants (in cm^{-1}) for the cold bands of $^{16}\text{O}^{12}\text{C}^{18}\text{O}$ in the region 3800–8500 cm^{-1}

Band	Type	v_0^{b}	G_v	B_v	$D_v \times 10^7$	$H_v \times 10^{13}$	$J_{\text{MAX}}^{\text{c}}$	$P/Q/R$	n/N^{d}	$\text{RMS} \times 10^{3e}$	Ref.
Ground state ^a			0.0	0.36818450	1.18701	-0.015					
30003-00001	$\Sigma-\Sigma$	3856.765894(52)	3856.765894(52)	0.36730060(25)	1.3329(26)	6.10(73)	51//48		87/87	0.22	
30002-00001	$\Sigma-\Sigma$	3987.596130(80) 3987.5946(8)	3987.596130(80)	0.36822690(34) 0.3682316(53)	0.8780(32) 0.964(90)	8.03(82)	55//48 30//38		96/98 1.68	0.35	[18]
30001-00001	$\Sigma-\Sigma$	4167.90648(21) 4167.9063(4)	4167.90648(21)	0.3694649(14) 0.369472(20)	0.604(19) 0.673(92)		28//26 30//26		42/45 0.86	0.56	[18]
00021-00001	$\Sigma-\Sigma$	4639.501233(74) 4639.5031(5)	4639.501233(74)	0.36239123(10) 0.3623912(15)	1.18055(25) 1.19(11)		69//59 46//46		123/125 2.19	0.45	[18] [20]
			4639.50154(3)	0.36239108(6)	1.18011(52)	0.31(12)				0.07	[19]
20013-00001	$\Sigma-\Sigma$	4791.25884(8) 4791.2597(9)	4791.25884(8)	0.36576078(23) 0.3657582(15)	1.5968(16) 1.579(4)	4.43(28)	64//61 64//42		121/121 4.44	0.37	[18]
			4791.25921(2)	0.36576046(3)	1.59379(21)	3.573(36)				0.06	[19]
20012-00001	$\Sigma-\Sigma$	4904.85842(12) 4904.8613(2)	4904.85842(12)	0.36484708(30) 0.3648432(87)	1.1250(16) 1.099(7)	12.51(23)	68//71 56//55		129/132 1.00	0.65	[18]
			4904.85920(3)	0.36484495(7)	1.10772(47)	8.993(87)				0.10	[19]
20011-00001	$\Sigma-\Sigma$	5042.581338(63) 5042.5835(8)	5042.581338(63)	0.36613211(18) 0.3661323(20)	0.8620(12) 0.866(17)	2.24(20)	62//64 42//43		120/120 3.83	0.32	[18]
			5042.58137(3)	0.36613269(8)	0.86704(60)	3.052(13)				0.10	[19]
10022-00001	$\Sigma-\Sigma$	5858.024337(79) 5858.0279(1)	5858.024337(79)	0.36250109(16) 0.3625010(2)	1.37836(62) 1.395(9)		54//54 47//49		105/107 0.36	0.43	[18]
10021-00001	$\Sigma-\Sigma$	5959.95282(11) 5959.9564(1)	5959.95282(11)	0.36262974(26)	1.0032(11)		53//50 45//46		99/99 21/60	0.59 0.44	[18]
			5959.954556(91)	0.36262836(17)	1.018(8) 0.99690(52)					0.38	[21]
30014-00001	$\Sigma-\Sigma$	5993.58182(11) 5993.5856(1)	5993.58182(11)	0.36635460(38) 0.366355(67)	1.8061(31) 1.817(8)	7.20(68)	58//56 50//51		95/102 43//62	0.47 0.91	[18] [21]
			5993.58314(19)	0.36635531(62)	1.8069(46)						

30013–00001	$\Sigma-\Sigma$	6127.779818(72) 6127.7834(3)	6127.779818(72) 0.36451673(21) 0.3645188(10)	1.3887(14) 1.407(8)	12.88(26)	64//62 54//58 //69	123/126	0.35 1.29 2.23	[18] [13]
		6127.78720(63)	6127.78720(63) 0.36450242(80) 6127.78244(28) 0.36451557(68) 6127.78094(9) 0.36457805(30)	1.3051(18) 1.3854(40) 1.4043(39)	16.8(13)	66//67	57//58	1.06 0.16	[21] [19]
30012–00001	$\Sigma-\Sigma$	6254.590215(72) 6254.5942(2)	6254.590215(72) 0.36528465(24) 0.365286(93)	0.8479(18) 0.865(9)	4.19(36)	58//59 42//54 64//69	118/118	0.36 1.01 1.47	[18] [13]
		6254.59187(26)	6254.59187(26) 0.36528197(36) 6254.59119(9) 0.36528466(23)	0.82438(90) 0.8414(16)			110/116	0.21	[19]
30011–00001	$\Sigma-\Sigma$	6429.17193(13) 6429.1763(2) 6429.17274(27)	6429.17193(13) 0.36663417(61) 0.366633(52) 6429.17274(27) 0.36663014(54)	0.6420(67) 0.623(3) 0.6006(19)	10.2(19)	48//49 43//42 49//56	94/98 95/97	0.55 0.68 1.48	[18] [13]
00031–00001	$\Sigma-\Sigma$	6922.195633(66) 6922.2022(8)	6922.195633(66) 0.35949795(10) 0.3594928(22) 6922.19697(8) 0.3594972(29)	1.17877(26) 1.169(9) 1.1737(43)	60//65 3.2(16)		119/119	0.40 2.62 0.17	[18] [19]
40014–00001	$\Sigma-\Sigma$	7338.77494(40)	7338.77494(40) 7465.09716(26)	0.3647278(18) 0.36431523(94)	1.674(15) 0.8738(62)	34//35 35//40	42/44 70/70	1.25 1.14	
40013–00001*	$\Sigma-\Sigma$	8120.10100(12)	8120.10100(12) 0.35970450(38)	1.3951(21)		50//39 42//36	84/88	0.60 1.26	[18]
		8120.1086(3)		0.3597037(10)	1.398(8)				
10031–00001	$\Sigma-\Sigma$	8220.35692(14) 8220.3643(2)	8220.35692(14) 0.35968143(39) 0.359682(91)	0.9918(20) 1.004(7)		48//41 33//37	90/90 0.88	0.70 0.88	[18]
01121e–00001e	$\Pi-\Sigma$	5277.15315(18)	5277.51601(18) 0.36286192(52) 0.3628716(47)	1.2027(28) 1.256(61)		38//45	73/75	0.79	[18]
01121f–00001f	$\Pi-\Sigma$	5277.15345(26)	5277.51683(26) 0.338470(82) 0.3633943(26)	1.2068(50) 1.203(14)		/41/ /22/	37/37	0.71	[18]

The uncertainties are given in parentheses in the unit of the last quoted digit. The bands with ^{**} are newly observed, but the corresponding upper states were observed through the cold bands in [18]. The 40013 state was observed through the hot band 40013–10002 in [21].

^a The parameters for the ground vibrational states are taken from [23].

^b v_0 is the band center.

^c J_{MAX} is the maximum value of the angular momentum quantum number observed for $P/Q/R$ branches.

^d n is the number of fitted line positions and N is the total number of assigned lines.

^e RMS is the root mean squares of the fitting residuals in cm^{-1} .

Table 3
Spectroscopic constants (in cm^{-1}) for the hot bands of $^{16}\text{O}^{12}\text{C}^{18}\text{O}$ in the region 3800–8500 cm^{-1}

Band	Type	v_0^{b}	ΔG_v	G_v	B_v	$D_v \times 10^7$	$H_v \times 10^{13}$	$J_{\text{MAX}}^{\text{c}}$	$P/Q/R$	n/N^{d}	RMS $\times 10^{3\text{c}}$	Ref.
01101e ^a				662.37335	0.36860192	1.20678	0.186					
01101f ^a				662.37335	0.36915234	1.20692	-0.285					
02201e ^a				1325.141	0.36956416	1.24872	-3.814					
02201f ^a				1325.141	0.36956416	1.23158	0.603					
22213e–02201e	$\Delta-\Delta$	4703.89751(37)	4703.88727(37)	6029.02827(37)	0.3670032(25)	0.476(32)		29//26		32/32	0.89	
22213f–02201f	$\Delta-\Delta$	4703.89752(36)	4703.88728(36)	6029.02828(36)	0.3670031(24)	0.456(32)		29//26		32/32	0.88	
30014–10002*	$\Sigma-\Sigma$	4734.15923(26)	4734.15923(26)	5993.58443(26)	0.3663520(12)	1.770(11)		32//32		34/35	0.55	
21113e–01101e	$\Pi-\Pi$	4743.69688(12)	4743.69418(12)	5406.06753(12)	0.36590175(25)	1.42598(96)		54//51		77/85	0.52	
		4743.6980(8)			0.3658992(25)	1.347(14)		47//43			3.90	[18]
				5406.06905(8)	0.36590221(21)	1.4303(23)	1.44(65)				0.14	[19]
21113f–01101f	$\Pi-\Pi$	4743.69657(13)	4743.69438(13)	5406.06773(13)	0.36697290(27)	1.5434(10)		52//53		78/83	0.59	
		4743.6965(5)			0.3669917(16)	1.592(9)		50//48			2.29	[18]
				5406.06885(8)	0.36697455(22)	1.5545(26)	1.10(81)				0.13	[19]
30013–10001*	$\Sigma-\Sigma$	4761.93596(92)	4761.93596(92)	6127.77939(92)	0.3645348(51)	1.579(59)		23//27		19/19	0.12	
30013–10002*	$\Sigma-\Sigma$	4868.35689(18)	4868.35689(18)	6127.78209(18)	0.36451564(73)	1.3684(52)		39//39		49/50	0.67	
30012–10001*	$\Sigma-\Sigma$	4888.74879(23)	4888.74879(23)	6254.59222(23)	0.36528482(79)	0.8490(52)		41//37		40/40	0.73	
22212e–02201e	$\Delta-\Delta$	4885.93241(23)	4885.92062(23)	6211.06162(23)	0.3666161(10)	1.2713(87)		36//34		40/44	0.69	
22212f–02201f	$\Delta-\Delta$	4885.93243(25)	4885.92064(25)	6211.06164(25)	0.3666159(11)	1.2527(93)		36//34		40/44	0.74	
21112e–01101e	$\Pi-\Pi$	4896.19186(12)	4896.18855(12)	5558.56190(12)	0.36529199(24)	1.15762(85)		56//53		81/90	0.52	
		4896.1956(20)			0.365215(17)	1.24(34)		//36			5.49	[18]
				5558.56448(6)	0.36529023(16)	1.1414(15)	3.48(40)				0.12	[19]
21112f–01101f	$\Pi-\Pi$	4896.191616(90)	4896.188752(90)	5558.562102(90)	0.36628862(18)	1.15662(63)		56//53		82/91	0.39	
		4896.1914(7)			0.3663102(34)	1.233(22)		20//35			2.62	[18]
				5558.56439(6)	0.36628847(14)	1.1558(13)	0.84(33)				0.12	[19]
30012–10002*	$\Sigma-\Sigma$	4995.16640(51)	4995.16640(51)	6254.59160(51)	0.3652824(23)	0.803(21)		32//32		27/29	1.04	
30011–10001*	$\Sigma-\Sigma$	5063.33021(52)	5063.33021(52)	6429.17364(52)	0.3666316(43)	0.588(59)		27//16		22/23	1.01	
21111e–01101e	$\Pi-\Pi$	5064.65596(16)	5064.65331(16)	5727.02666(16)	0.36595980(36)	1.0184(15)		51//48		83/89	0.69	
		5064.6543(9)		5727.02840(9)	0.3659652(51)	0.911(51)	4.41(105)	32//			1.60	[18]
					0.36595947(28)	1.0232(33)					0.15	[19]
21111f–01101f	$\Pi-\Pi$	5064.65604(12)	5064.65403(12)	5727.02738(12)	0.36713957(31)	0.9640(14)		49//47		75/79	0.52	
		5064.6561(8)			0.3671602(30)	1.029(24)					2.16	[18]
				5727.02858(9)	0.36714004(29)	0.9696(36)	1.99(123)	38//			0.13	[19]

22211e-02201e	$\Delta-\Delta$	5080.43830(40)	5080.42845(40)	6405.56945(40)	0.3671012(36)	1.426(66)	25//24	21/23	0.72	
22211f-02201f ^f	$\Delta-\Delta$	5080.43831(40)	5080.42846(40)	6405.56946(40)	0.3671011(36)	1.405(66)	25//24	21/23	0.71	
11122e-01101e	$\Pi-\Pi$	5813.43660(60) 5813.3835(117)	5813.43091(60)	6475.80426(60)	0.3629110(24) 0.36386(23)	1.287(19)	36//32	41/53	1.29 22.9	[18]
11122f-01101f ^f	$\Pi-\Pi$	5813.43285(72) 5813.4454(119)	5813.42739(72)	6475.80074(72)	0.3636921(30) 0.36410(23)	1.417(27)	34//29	39/45	1.35 13.1	[18]
31114e-01101e	$\Pi-\Pi$	5935.33097(82) 5935.3232(98)	5935.33097(82)	6597.70432(82)	0.3663396(53) 0.367103(70)	-1.698(71) 3.1(10)	27//24 27//27	20/27	0.89 16.5	[18]
31114f-01101f ^f	$\Pi-\Pi$	5935.32778(79) 5935.3305(81)	5935.32778(79)	6597.70113(79)	0.3675917(44) 0.366947(58)	1.783(49) 1.03(87)	27//28 29//29	22/31	1.12 13.3	[18]
11121e-01101e	$\Pi-\Pi$	5956.18389(59)	5956.18389(59) 5956.18457(62)	6618.55724(59) 6618.55792(62)	0.3628811(26) 0.3628758(31)	1.141(24) 1.063(32)	31//31 //30	22/26	0.87 0.69	[21]
11121f-01101f ^f	$\Pi-\Pi$	5956.18522(74)	5956.18522(74) 5956.18314(47)	6618.55857(74) 6618.55649(47)	0.3636637(27) 0.3636717(17)	1.208(20) 1.052(11)	28//35 //38	24/25	1.24 0.79	[21]
31113e-01101e	$\Pi-\Pi$	6100.30174(24)	6100.30174(24) 6100.30124(34)	6762.67509(24) 6762.67459(34)	0.3649743(14) 0.3649816(12)	1.054(20) 1.1644(74)	44//40 49//36	67/73	0.77 1.16	[21]
31113f-01101f ^f	$\Pi-\Pi$	6100.30063(20)	6100.30063(20) 6100.30102(47)	6762.67398(20) 6762.67437(47)	0.3661937(13) 0.3661995(11)	1.168(22) 1.2561(47)	39//38 51//34	69/72	0.58 1.76	[21]
31112e-01101e	$\Pi-\Pi$	6265.20659(28)	6265.20659(28) 6265.20578(52)	6927.57994(28) 6927.94445(52)	0.3653154(11) 0.3653219(26)	0.9110(89) 0.948(23)	38//33 37//49	53/59	0.88 1.64	[13]
31112f-01101f ^f	$\Pi-\Pi$	6265.20191(59)	6265.20191(59) 6265.20621(76)	6927.57526(59) 6927.94617(76)	0.3666666(50) 0.3666136(38)	2.02(10) 0.710(35)	794(58) 48//45	54/59	1.55 2.08	[13]
01131e-01101e ^f	$\Pi-\Pi$	6885.15520(29)	6885.14659(29) 6885.1589(19)	7547.52014(29)	0.35999143(71) 0.360018(13)	1.1877(29)	50//49	65/82	1.15 2.64	[18]
01131f-01101f ^a	$\Pi-\Pi$	6885.15071(35)	6885.14207(35) 6885.1559(16)	7547.51562(35)	0.36050742(95) 0.360670(21)	1.2098(46) 2.31(45)	48//42	64/81	1.32 3.78	[18]

The uncertainties are given in parentheses in the unit of the last quoted digit. For the three $\Delta-\Delta$ bands, the lines of the $e-e$ and $f-f$ sub-bands which have the same J value are not resolved. So we use the overlapped lines to calculate the constants of the upper energy levels for both the $e-e$ and $f-f$ sub-bands. The bands with “*” are newly observed, but the corresponding upper states were observed through the cold bands in [18].

^a Parameters taken from [23].

^b v_0 is the band center.

^c J_{MAX} is the maximum value of the angular momentum quantum number observed for $P/Q/R$ branches.

^d n is the number of fitted line positions and N is the total number of assigned lines.

^e RMS is the root mean squares of the fitting residuals in cm^{-1} .

^f The R27-R35 lines of 01131-01101 band are overlapped with the strong P23-P25 lines of 00031-00001 band.

state and the 01101e and 01101f vibrational states) have been fixed to the literature values [23] ($^{12}\text{C}^{18}\text{O}_2$ and $^{16}\text{O}^{12}\text{C}^{18}\text{O}$). Here the vibrational levels are labeled using the HITRAN notation [22].

3.1. $^{16}\text{O}^{12}\text{C}^{18}\text{O}$

On the basis of combination differences, nineteen cold bands and eighteen hot bands can be assigned to the $^{16}\text{O}^{12}\text{C}^{18}\text{O}$ species. Among them, three cold bands and nine hot bands are newly observed. The corresponding upper vibrational states of hot bands observed here (30014–10002, 30013–10001, 30003–10002, 30012–10002, 30012–10001 and 30011–10001) were reported through the cold bands in Ref. [18]. The upper state of the cold band 40013–00001 observed here was also reported through the hot band 40013–10002 [21]. For three observed Δ - Δ bands, the lines of e and f sub-bands with the same J values are overlapped and cannot be separated in the spectrum. So

we just use the overlapped lines to fit the constants of the upper energy levels for both the e and f sub-bands. The vibrational assignment of newly observed bands is straightforward with the predictions based on the effective Hamiltonian model [8,24].

In Tables 2 and 3, the fitted values of the spectroscopic constants of all observed bands are presented. Full list of the assigned transitions are available as [Supplementary materials](#) attached to this paper. Fourteen cold bands and five hot bands in this region were previously reported by Mandin [18]. As a comparison, the spectroscopic parameters from Ref. [18] are also presented in those Tables. They are in good agreement with our measurements. Owing to the better spectral resolution applied in our measurement and to the higher concentration of $^{16}\text{O}^{12}\text{C}^{18}\text{O}$ in our sample, more rotational transitions are observed and it leads to probably more reliable parameter values. The improvement of the rotational parameters is very prominent for the 11122 and 31114 states. For these

Table 4
Spectroscopic constants (in cm^{-1}) for the cold bands of $^{12}\text{C}^{18}\text{O}_2$ in the region 3800–8500 cm^{-1}

Band	Type	v_0^{b}	G_v	B_v	$D_v \times 10^7$	H_v	$J_{\text{MAX}}^{\text{c}} P/Q/R$	n/N^{d}	$\text{RMS} \times 10^{3\text{e}}$	Ref.
Ground state ^a			0.0	0.34681727	1.05368					
20013–00001	$\Sigma-\Sigma$	4721.92229(36)	4721.92229(36)	0.34400647(35)	1.34751(62)		80/78	79/79	1.71	[19]
			4721.92089(2)	0.34401234(3)	1.37645(13)	3.376(17)				
20012–00001	$\Sigma-\Sigma$	4833.25379(28)	4833.25379(28)	0.34393993(58)	0.8637(22)		56/54	54/56	1.07	[19]
			4833.25341(3)	0.34394665(9)	0.92943(99)	14.56(31)				
20011–00001	$\Sigma-\Sigma$	4989.23501(18)	4989.23501(18)	0.34525786(18)	0.75674(32)		74/82	72/73	0.88	[19]
			4989.23428(3)	0.34526138(5)	0.77886(36)	3.249(69)				
30014–00001	$\Sigma-\Sigma$	5903.03931(15)	5903.03931(15)	0.34443203(21)	1.53460(55)		64/66	65/65	0.65	[19]
			5903.03983(9)	0.34443537(30)	1.5599(35)	4.18(109)				
30013–00001	$\Sigma-\Sigma$	6024.50505(24)	6024.50505(24)	0.34331685(38)	1.0065(11)		68/72	61/70	1.00	[19]
			6024.50413(5)	0.34332255(11)	1.05092(97)	8.14(23)				
30012–00001	$\Sigma-\Sigma$	6166.62429(16)	6166.62429(16)	0.34459853(22)	0.75033(52)		70/62	65/65	0.71	[19]
			6166.62501(10)	0.34460053(22)	0.7611(13)					
30011–00001	$\Sigma-\Sigma$	6359.57104(18)	6359.57104(18)	0.34578836(30)	0.51502(96)		56/60	57/57	0.73	[19]
		00031–00001	6868.97793(13)	0.33864442(15)	1.04798(31)		66/76	69/70	0.61	
			6868.97851(5)	0.33864398(12)	1.0463(12)	-0.85(29)				
40015–00001	$\Sigma-\Sigma$	7069.72679(41)	7069.72679(41)	0.3449344(14)	1.7290(87)		32/38	25/26	0.74	
40014–00001	$\Sigma-\Sigma$	7209.00876(25)	7209.00876(25)	0.34305002(50)	1.2646(18)		50/54	49/49	0.89	
40013–00001	$\Sigma-\Sigma$	7341.52752(20)	7341.52752(20)	0.34379562(45)	0.7293(18)		52/50	47/49	0.71	
40012–00001	$\Sigma-\Sigma$	7522.32345(96)	7522.32345(96)	0.3451875(44)	0.460(40)		32/32	27/29	1.95	
10032–00001	$\Sigma-\Sigma$	8041.529806(95)	8041.529806(95)	0.33855537(19)	1.19776(65)		58/40	49/49	0.37	
10031–00001	$\Sigma-\Sigma$	8147.51607(13)	8147.51606(13)	0.33913281(25)	0.89572(84)		58/54	54/55	0.53	
01121e–00001	$\Pi-\Sigma$	5236.55477(11)	5236.55477(11)	0.34182481(19)	1.06250(58)		50/60	55/55	0.46	
01121f–00001	$\Pi-\Sigma$	5236.55469(27)	5236.55469(27)	0.34229486(42)	1.0704(11)		/62/	31/31	0.78	
11122e–00001	$\Pi-\Sigma$	6409.30905(26)	6409.30905(26)	0.34170658(58)	1.1504(22)		34/52	39/39	0.85	
11122f–00001	$\Pi-\Sigma$	6409.30878(46)	6409.30878(46)	0.34235923(84)	1.2020(29)		/56/	26/27	1.23	
11121e–00001	$\Pi-\Sigma$	6558.03762(27)	6558.03762(27)	0.34205614(64)	0.9753(25)		30/52	39/39	0.93	
11121f–00001	$\Pi-\Sigma$	6558.03745(20)	6558.03745(20)	0.34280952(54)	0.9539(27)		/46/	23/23	0.49	

The uncertainties are given in parentheses in the unit of the last quoted digit.

^a The parameters for the ground vibrational states are taken from [23].

^b v_0 is the band center.

^c J_{MAX} is the maximum value of the angular momentum quantum number observed for $P/Q/R$ branches.

^d n is the number of fitted line positions and N is the total number of assigned lines.

^e RMS is the root mean squares of the fitting residuals in cm^{-1} .

states the parameters derived from the Venus spectra gave very large RMS values.

We also compared our data with the work of Majcherova et al. [13] and Perevalov et al. [21] where the CW cavity ring down spectroscopy studies of the carbon dioxide bands near 1.5 μm were reported. Because of the very high sensitivity of the CW-CRDS method, more weak lines near 1.5 μm were observed there. But our FTS spectrum may give more accurate line position for those relatively stronger lines. It is partly owing to the usage of O-18 enriched sample in our measurements, while natural CO₂ sample were used in the CW-CRDS measurements [13,21], the ¹⁶O¹²C¹⁸O lines could be blended by much stronger lines of ¹⁶O¹²C¹⁶O and ¹⁶O¹³C¹⁶O.

There are thirteen cold bands and four hot bands listed in the HITRAN-04 database [22] in this region. Many of our observed line positions are close to those listed in HITRAN. But for some bands, large differences can be found. For example, the deviation changes from 0.1 to –0.1 cm^{−1} when the *J* value increases from 3 to 43 for the 30003–00001 band. And for the 21112–01101 band, the difference is not very large for the lines of the *f*–*f* sub-band, but increases from 0.002 up to 0.257 cm^{−1} when the *J* value increases from 2 to 50 for the lines of *e*–*e* sub-band. The same phenomenon happens in the 21111–01101 band, while the differences are not so large. Note that the line positions of the above discussed bands listed in HITRAN were derived by the DND (direct numerical diagonalization) calculations [25].

3.2. ¹²C¹⁸O₂

On the basis of the combination differences, 17 cold bands and 9 hot bands can be assigned to the ¹²C¹⁸O₂ species (fourteen Σ – Σ and three Σ – Π cold bands, nine Π – Π hot bands). Rotational levels with *J* value up to 82 have been observed. The vibrational assignment has been performed with the help of the predictions performed with the preliminary set of parameters of the global effective vibration–rotation Hamiltonian which will be discussed in Section 4.

The spectroscopic parameters *G_v*, *B_v* and *D_v* have been fitted to the line positions of all observed bands of ¹²C¹⁸O₂. The RMS deviations of the fits are less than 0.001 cm^{−1} for not very weak bands, close to the experimental uncertainty, but slightly larger (about 0.002 cm^{−1}) for the weak bands. Full list of the assigned rotational lines are available as Supplementary materials attached to the paper. In Tables 4 and 5 we present the fitted values of the spectroscopic constant for the observed cold and hot bands, respectively. For comparison, we present in italic the respective spectroscopic constants obtained in the recent paper [19]. Our spectroscopic constants are in good agreement with that from Ref. [19]. There is only a minor exception: in our case the centrifugal distortion constants *H_b* are not significant. In total we have managed to assign fourteen additional bands compared to Ref. [19].

4. Global fit the rovibrational levels of ¹²C¹⁸O₂

The polyad model of the global effective Hamiltonian suggested by Chedin [24] and developed by Teffo et al. [1,4] has been used in the fitting of the ro-vibrational transitions. There are approximate relations between the harmonic frequencies of CO₂:

$$\omega_1 \approx 2\omega_2, \quad \omega_3 \approx 3\omega_2. \quad (2)$$

As a result, the vibrational states can be grouped in to vibrational polyads with the quantum number *P*:

$$P = 2V_1 + V_2 + 3V_3. \quad (3)$$

The effective Hamiltonian within the framework of the polyad model takes into account three types of the accidental resonance interactions: anharmonic, Coriolis resonance and anharmonic + ℓ -type resonance interactions. All matrix elements of this Hamiltonian up to the sixth-order terms and notations are presented in Refs. [1,4].

The list-square fittings of the effective Hamiltonian parameters to the observed line positions have been performed using the GIP computer code [6,26]. It minimizes the dimensionless weighted standard deviation which is defined as:

$$\chi = \sqrt{\frac{\sum_i [(v_i^{\text{obs}} - v_i^{\text{calc}})/\epsilon^k]^2}{N - n}}, \quad (4)$$

where v_i^{obs} and v_i^{calc} are the observed and calculated wave-numbers, *N* is the number of fitted transitions, *n* is the number of adjusted parameters, and ϵ^k is the experimental uncertainty of the spectrum (index *k*). Before the fitting, all the collected data were checked for the consistency using the Ritz principle (see, for example, Ref. [13]). Some calibration factors were used to correct the observed line positions.

To characterize the quality of the fit, we use the root mean squares of the residuals which is defined as

$$\text{RMS} = \sqrt{\frac{1}{N} \sum_i (v_i^{\text{obs}} - v_i^{\text{calc}})^2}. \quad (5)$$

In the fit we have used 5443 line positions of 73 bands from those observed in this work and collected from the literatures [18,19,27–33]. They are summarized in Table 6. The calibration factors used in this work were derived as the result of the term value analysis performed for all the isotopic species of carbon dioxide. For details see Ref. [6]. The total number of the collected transitions was 5530 but 51 lines were rejected by Ritz computer code, 3 Venus lines were excluded from the fit because of the overlap with strong lines, and 31 lines were excluded from the fit as outliers. Using the collected data we have managed to fit 65 parameters of the effective Hamiltonian. In the fitting we get the weighted standard deviation $\chi = 2.37$ and global RMS = 0.00145 cm^{−1}. The RMS values for respective experimental data sources are presented in Table 6, and the effective Hamiltonian

Table 5
Spectroscopic constants (in cm^{-1}) for the hot bands of $^{12}\text{C}^{18}\text{O}_2$ in the region 3800–8500 cm^{-1}

Band	Type	v_0^{b}	ΔG_v	G_v	B_v	$D_v \times 10^7$	$H_v \times 10^{13}$	$J_{\text{MAX}}^{\text{c}}$	$P/Q/R$	n/N^{d}	$\text{RMS} \times 10^{3e}$	Ref.
01101e ^a				657.331	0.34723371	1.07024						
01101 ^a				657.331	0.34772525	1.07696						
21113e–01101e	Π–Π	4674.24946(27)	4674.24659(27)	5331.58046(27) 5331.57675(5)	0.34436672(38) 0.34436372(10)	1.25294(98) 1.26236(89)	65//63 1.66(22)			59/60	1.07	[19]
21113f–01101f	Π–Π	4674.24972(24)	4674.24724(24)	5331.58072(24) 5331.57668(7)	0.34524454(32) 0.34524482(22)	1.34586(76) 1.3580(25)	70//64 1.46(72)			62/62	1.01	[19]
21112e–01101e	Π–Π	4827.25161(17)	4827.24865(17)	5484.58261(17) 5484.57890(5)	0.34426885(27) 0.34426455(11)	1.01944(77) 1.0180(10)	65//59 −0.18(26)			54/54	0.70	[19]
21112f–01101f	Π–Π	4827.25156(19)	4827.24901(19)	5484.58256(19) 5484.57885(5)	0.34517697(23) 0.34517562(13)	1.01773(52) 1.0218(14)	68//70 0.92(40)			61/62	0.79	[19]
21111e–01101e	Π–Π	5009.41854(28)	5009.41638(28)	5666.74954(28) 5666.74597(9)	0.34507845(42) 0.34507379(35)	0.9099(11) 0.9136(45)	67//63 1.6(15)			57/60	1.16	[19]
21111f–01101f	Π–Π	5009.41832(23)	5009.41679(23)	5666.74932(23) 5666.74592(9)	0.34620287(31) 0.34619960(29)	0.89163(82) 0.8868(33)	68//54 −0.29(97)			55/56	0.91	[19]
31114e–01101e	Π–Π	5842.85893(28)	5842.85621(28)	6500.18993(28)	0.34451848(55)	1.3630(19)	57//53			52/53	1.08	
31114f–01101f	Π–Π	5842.85899(28)	5842.85691(28)	6500.18999(28)	0.34564765(53)	1.4998(18)	54//56			51/52	1.05	
31113e–01101e	Π–Π	6002.18619(22)	6002.18281(22)	6659.51719(22)	0.34385216(43)	1.0659(15)	55//57			49/52	0.77	
31113f–01101f	Π–Π	6002.18587(27)	6002.18306(27)	6659.51687(27)	0.34491006(49)	1.1031(16)	56//56			51/52	0.97	
31112e–01101e	Π–Π	6177.35294(26)	6177.35021(26)	6834.68394(26)	0.34450384(56)	0.9260(21)	51//53			46/46	0.94	
31112f–01101f	Π–Π	6177.35300(19)	6177.35101(19)	6834.68400(19)	0.34573101(41)	0.9033(16)	50//52			48/49	0.69	
01131e–01101e	Π–Π	6832.30954(19)	6832.30143(19)	7489.64054(19) 7489.63691(32)	0.33912886(33) 0.33912810(91)	1.0588(10) 1.0847(69)	61//57			54/55	0.74	[19]
01131f–01101f	Π–Π	6832.30906(14)	6832.30091(14)	7489.64006(14) 7489.63646(36)	0.33958634(24) 0.33958692(98)	1.07126(66) 1.0783(78)	64//38			45/45	0.52	[19]
11132e–01101e	Π–Π	7985.66963(38)	7985.66147(38)	8643.00063(38)	0.3390719(14)	1.1645(93)	41//35			35/36	1.13	
11132f–01101f	Π–Π	7985.67221(60)	7985.66419(60)	8643.00321(60)	0.3397049(26)	1.133(21)	38//34			33/35	1.59	
11131e–01101e	Π–Π	8131.25392(69)	8131.24604(69)	8788.58492(69)	0.3393564(27)	1.009(21)	37//35			28/29	1.46	
11131f–01101f	Π–Π	8131.25502(76)	8131.24746(76)	8788.58602(76)	0.3400679(23)	0.966(14)	38//40			30/32	1.70	

The uncertainties are given in parentheses in the unit of the last quoted digit.

^a Parameters taken from [23].

^b v_0 is the band center.

^c J_{MAX} is the maximum value of the angular momentum quantum number observed for $P/Q/R$ branches.

^d n is the number of fitted line positions and N is the total number of assigned lines.

^e RMS is the root mean squares of the fitting residuals in cm^{-1} .

Table 6

Spectrum-by-spectrum analysis of the experimental data and statistics of the $^{12}\text{C}^{18}\text{O}_2$ global line positions fit

Reference	Calibration factor	Precision (in 10^{-3} cm $^{-1}$)	N_{fit}	RMS _{RITZ} (in 10^{-3} cm $^{-1}$)	RMS _{GIP} (in 10^{-3} cm $^{-1}$)
Maki et al. [27]	1.0 ^c	0.00033	98	0.000014	<0.0003
Bradley et al. [28]	1.0 ^c	0.001	84	0.00014	<0.0003
Siemsen [29]	1.0 ^c	0.033	41	0.011	0.043
Toth et al. [19]	1.000000010	0.3	1341	0.16	0.67
Bailly [30,31] (4.5 μm region)	0.999999770 ^b	0.5 ^a	1214	0.21	1.55
Bailly [32] (15 μm region)	1.0 ^d	0.5 ^a	117	0.40	1.06
Esplin et al. [33] (4.3 μm region)	0.999999655 ^b	0.5 ^a	535	0.76	1.45
Esplin et al. [33] (2.8 μm region)	0.999999688 ^b	0.5 ^a	136	0.64	1.25
Mandin [18]	0.999999372 ^b	2.0 ^a	20	1.88	2.08
This work	1.000000064	1.0	1856	0.66	1.88

 N_{fit} is the number of lines included in the fit.^a Experimental precision is set to a guessed value.^b Calibration factors from Ref. [13].^c Uncalibrated reference spectra.^d Could not be determined.

Table 7

The effective Hamiltonian parameters for $^{12}\text{C}^{18}\text{O}_2$

N	Parameter	Value (cm $^{-1}$)	Order	N	Parameter	Value (cm $^{-1}$)	Order
<i>Diagonal vibrational parameters</i>							
1	ω_1	1275.8655(140) ^a		14	y_{122} ^b	-0.23318	10^{-2}
2	ω_2	662.58697(43)		15	y_{123}	12.48(24)	10^{-2}
3	ω_3	2359.5211(35)		16	y_{133}	4.057(10)	10^{-2}
4	x_{11}	-2.48551(71)		17	y_{222}	-0.5990(47)	10^{-2}
5	x_{12}	-4.81759(71)		18	y_{223}	-2.859(57)	10^{-2}
6	x_{13}	-17.5510(94)		19	y_{233}	0.906(12)	10^{-2}
7	x_{22}	1.55293(16)		20	y_{333}	0.1161(11)	10^{-2}
8	x_{23}	-12.28525(43)		21	$y_{1\ell\ell}$	-0.554(25)	10^{-2}
9	x_{33}	-12.23929(16)		22	$y_{2\ell\ell}$	0.8571(57)	10^{-2}
10	$x_{\ell\ell}$ ^c	-0.9885909221		23	$y_{3\ell\ell}$	3.381(59)	10^{-2}
11	y_{111}	-0.2589(53)	10^{-2}	24	z_{2233}	6.49(29)	10^{-4}
12	y_{112}	-3.700(50)	10^{-2}	25	z_{2333}	3.764(37)	10^{-4}
13	y_{113}	-13.69(47)	10^{-2}	26	z_{3333}	3.0079(36)	10^{-4}
<i>Diagonal rotational and vibrational-rotational parameters</i>							
27	B_e	0.34802518(13)		35	γ_{33}	0.1011(23)	10^{-5}
28	α_1	1.00167(10)	10^{-3}	36	ε_{233}	0.2236(90)	10^{-6}
29	α_2	-0.67074(10)	10^{-3}	37	ε_{333}	0.0224(12)	10^{-6}
30	α_3	2.74434(10)	10^{-3}	38	D_e	0.1035857(97)	10^{-6}
31	γ_{12}	-0.889(16)	10^{-5}	39	β_2	1.8616(38)	10^{-9}
32	γ_{13}	-1.1732(85)	10^{-5}	40	β_3	-0.2111(56)	10^{-9}
33	γ_{22}	-0.4037(45)	10^{-5}	41	η_{13}	-2.19(87)	10^{-11}
34	γ_{23}	0.9933(36)	10^{-5}	42	H_e	0.91(11)	10^{-14}
<i>Parameters of ℓ-doubling matrix elements</i>							
43	L_e	-0.122892(62)	10^{-3}	45	L_2	0.205(39)	10^{-6}
44	L_1	-2.15(15)	10^{-6}	46	L_J	0.930(39)	10^{-10}
<i>Parameters of Fermi-interaction matrix elements</i>							
47	F_e	-25.52047(22)		54	F_{33}	-0.0416(86)	10^{-2}
48	F_1	0.29624(21)		55	$F_{\ell\ell}$	0.1327(21)	10^{-2}
49	F_2	0.31069(12)		56	F_J	0.112353(45)	10^{-3}
50	F_3	0.08838(57)		57	F_e^L	-0.6889(60)	10^{-5}
51	F_{11}	-0.2082(25)	10^{-2}	58	F_e^{IV}	0.6682(58)	10^{-2}
52	F_{12}	0.2466(60)	10^{-2}	59	F_J^{IV}	-0.1495(39)	10^{-6}
53	F_{23}	-0.446(14)	10^{-2}				
<i>Parameters of Coriolis-interaction matrix elements</i>							
60	C_e	-0.3289(10)	10^{-1}	63	C_J	0.756(68)	10^{-7}
61	C_1	0.724(42)	10^{-3}	64	C_{e1}	-0.2318(43)	10^{-2}
62	C_2	1.052(44)	10^{-3}	65	C_{e2}	0.380(12)	10^{-2}

^a Uncertainties in parentheses represent one standard deviation in units of the last quoted digit.^b Fixed value.^c Fixed to the value given by Chedin [24].

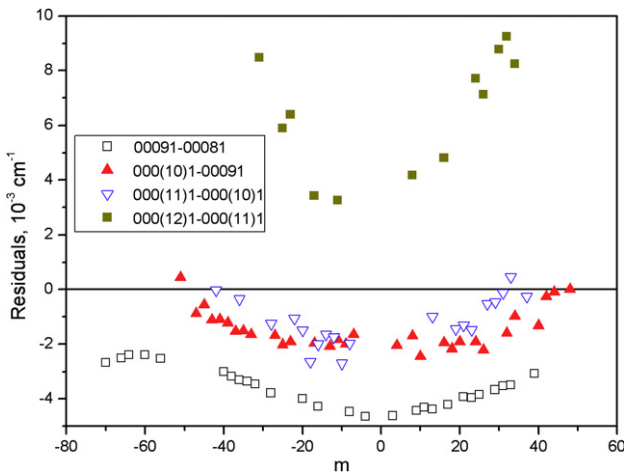


Fig. 3. The residuals between the observed [30,31] and calculated line positions for the 00091–00081, 000(10)1–00091, 000(11)1–000(10)1 and 000(12)1–000(11)1 bands.

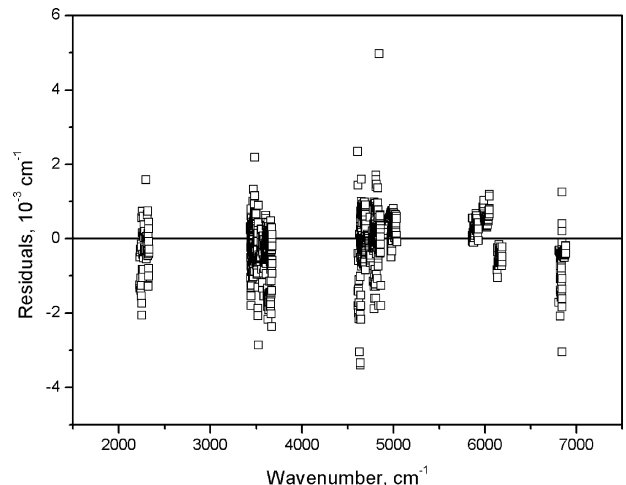


Fig. 5. The residuals between our calculated line positions and those observed in [19].

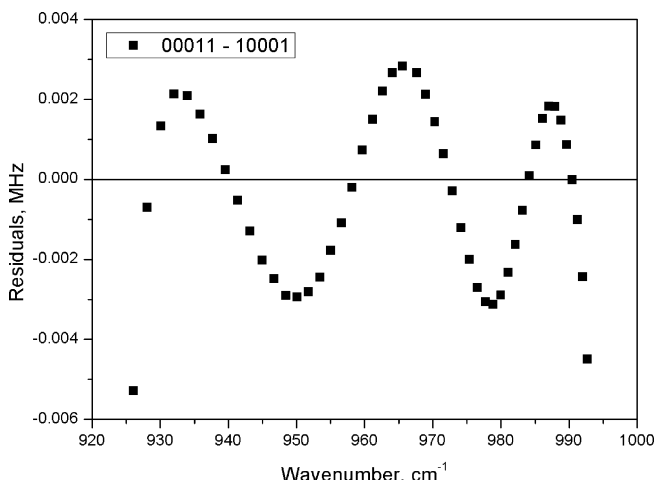


Fig. 4. The residuals between the values of the secondary frequency standards relating to the 00011–10001 band [27] and our calculated values. The uncertainty of the secondary frequency standards is 10^{-2} MHz.

parameters obtained from the fit are given in Table 7. The weighted standard deviation values show that we have almost reached the experimental accuracy. It should be noted that the standard deviation values could be overestimated because we used estimated values for the precisions of several experimental data sources. As for the experimental line positions provided in this work, the accuracy is estimated to be 0.001 cm^{-1} for unblended lines but a number of blended lines were also weighted assuming the same accuracy. The standard deviations of the bands $000(V_3 + 1)1 - 000V_31$ are relatively large for high V_3 values. The residuals of four such kind bands are illustrated in Fig. 3. One reason for the large residuals for the 000(12)1–000(11)1 band could be that the very weak lines of this band are blended with the very strong lines of other bands. The obtained effective Hamiltonian parame-

ters can reproduce the secondary standards of frequencies suggested in Ref. [27] within their uncertainties. As an example, we present in Fig. 4 the residuals between the values of the secondary frequency standards associated to the 00011–10001 band [27] and our calculated values. Finally, in Fig. 5 we give the residuals between the values of the line positions presented in the recent paper [19] and our calculated ones.

5. Conclusion

In this paper we present the results of the extensive measurements of the line positions of the $^{16}\text{O}^{12}\text{C}^{18}\text{O}$ and $^{12}\text{C}^{18}\text{O}_2$ isotopic species of carbon dioxide in the $3800\text{--}8500\text{ cm}^{-1}$ region. Seventeen cold bands and nine hot bands of $^{12}\text{C}^{18}\text{O}_2$, nineteen cold bands and eighteen hot bands of $^{16}\text{O}^{12}\text{C}^{18}\text{O}$ are reported. The uncertainty of the line position determination is estimated to be better than 0.001 cm^{-1} for unblended lines. The spectroscopic parameters G_v , B_v , and D_v , have been determined for all observed bands. The observed line positions together with those collected from the literatures allowed us to determine 65 effective Hamiltonian parameters which reproduce the line positions of all observed bands of $^{12}\text{C}^{18}\text{O}_2$ with RMS = 0.00145 cm^{-1} . The obtained results will be used for the development of CDSD databank [34].

Acknowledgments

This work is jointly supported by NSFC-China (Grant Nos. 20473079 and 10574124) and RFBR-Russia (Grant No. 06-05-39016), and by the Fok Ying Tong Education Foundation (101013). Dr. F. Qi in NSRL (Hefei) is acknowledged for PIMS measurements. Perevalov and Tashkun thank R.A. Toth and his colleagues for providing their measured line parameters of $^{12}\text{C}^{18}\text{O}_2$.

Appendix A. Supplementary data

Supplementary data for this article are available on ScienceDirect (www.sciencedirect.com) and as part of the Ohio State University Molecular Spectroscopy Archives (http://msa.lib.ohio-state.edu/jmsa_hp.htm).

References

- [1] J.-L. Teffo, O.N. Sulakshina, V.I. Perevalov, *J. Mol. Spectrosc.* 156 (1992) 48.
- [2] V.I. Perevalov, E.I. Lobodenko, O.M. Lyulin, J.-L. Teffo, *J. Mol. Spectrosc.* 171 (1995) 435.
- [3] J.-L. Teffo, O.M. Lyulin, V.I. Perevalov, E.I. Lobodenko, *J. Mol. Spectrosc.* 187 (1998) 28.
- [4] S.A. Tashkun, V.I. Perevalov, J.-L. Teffo, L.S. Rothman, Vl.G. Tyuterev, *J. Quant. Spectrosc. Radiat. Transfer* 60 (1998) 785.
- [5] S.A. Tashkun, V.I. Perevalov, J.-L. Teffo, Vl.G. Tyuterev, *J. Quant. Spectrosc. Radiat. Transfer* 62 (1999) 571.
- [6] S.A. Tashkun, V.I. Perevalov, J.-L. Teffo, M. Lecoutre, T.R. Huet, A. Campargue, D. Bailly, M.P. Esplin, *J. Mol. Spectrosc.* 200 (2000) 162.
- [7] J.-L. Teffo, C. Claveau, Q. Kou, G. Guelachvili, A. Ubelmann, V.I. Perevalov, S.A. Tashkun, *J. Mol. Spectrosc.* 201 (2000) 249.
- [8] S.A. Tashkun, V.I. Perevalov, J.-L. Teffo, *J. Mol. Spectrosc.* 210 (2001) 137.
- [9] J.-L. Teffo, L. Daumont, C. Claveau, A. Valentin, S.A. Tashkun, V.I. Perevalov, *J. Mol. Spectrosc.* 213 (2002) 145.
- [10] J.-L. Teffo, L. Daumont, C. Claveau, A. Valentin, S.A. Tashkun, V.I. Perevalov, *J. Mol. Spectrosc.* 219 (2003) 271.
- [11] Y. Ding, V.I. Perevalov, S.A. Tashkun, J.-L. Teffo, A.-W. Liu, S.-M. Hu, *J. Mol. Spectrosc.* 222 (2003) 276.
- [12] Y. Ding, P. Macko, D. Romanini, V.I. Perevalov, S.A. Tashkun, J.-L. Teffo, S.-M. Hu, A. Campargue, *J. Mol. Spectrosc.* 226 (2004) 146.
- [13] Z. Majcherova, P. Macko, D. Romanini, V.I. Perevalov, S.A. Tashkun, J.-L. Teffo, A. Campargue, *J. Mol. Spectrosc.* 230 (2005) 1.
- [14] L. Wang, V.I. Perevalov, S.A. Tashkun, A.-W. Liu, S.-M. Hu, *J. Mol. Spectrosc.* 233 (2005) 297.
- [15] L. Wang, V.I. Perevalov, S.A. Tashkun, Y. Ding, S.-M. Hu, *J. Mol. Spectrosc.* 234 (2005) 84.
- [16] J. Vander Auwera, C. Claveau, J.-L. Teffo, S.A. Tashkun, V.I. Perevalov, *J. Mol. Spectrosc.* 235 (2006) 77.
- [17] B.V. Perevalov, S. Kassi, D. Romanini, V.I. Perevalov, S.A. Tashkun, A. Campargue, *J. Mol. Spectrosc.* 241 (2007) 90.
- [18] J.-Y. Mandin, *J. Mol. Spectrosc.* 67 (1977) 304.
- [19] R.A. Toth, C.E. Miller, L.R. Brown, V. Malathy Devi, D.C. Benner, *J. Mol. Spectrosc.* 243 (2007) 43.
- [20] R.J. Kshirsagar, L.P. Giver, C. Chackerian Jr., L.R. Brown, *J. Quant. Spectrosc. Radiat. Trans.* 61 (1999) 695.
- [21] B.V. Perevalov, S. Kassi, D. Romanini, V.I. Perevalov, S.A. Tashkun, A. Campargue, *J. Mol. Spectrosc.* 238 (2006) 241.
- [22] L.S. Rothman, D. Jacquemart, A. Barbe, D.C. Benner, M. Birk, L.R. Brown, M.R. Carleer, C. Chakerian Jr., K.V. Chance, V. Dana, V.M. Devi, J.-M. Flaud, R.R. Gamache, A. Goldman, J.-M. Hartmann, K.W. Jucks, A. Maki, J.-Y. Mandin, S.T. Massie, J. Orphal, A. Perrin, C.P. Rinsland, M.A.H. Smith, J. Tennysson, R.N. Tolchenov, R.A. Toth, J. Vander Auwera, P. Varanasi, G. Wagner, *J. Quant. Spectrosc. Radiat. Transfer* 96 (2005) 139.
- [23] L.S. Rothman, R.L. Hawkins, R.B. Wattson, R.R. Gamache, *J. Quant. Spectrosc. Radiat. Transfer* 48 (1992) 537.
- [24] A. Chedin, *J. Mol. Spectrosc.* 76 (1979) 430.
- [25] R.B. Wattson, L.S. Rothman, *J. Quant. Spectrosc. Radiat. Transfer* 48 (1992) 763.
- [26] S.A. Tashkun, Vl.G. Tyuterev, in: A.I. Nadezhinskii, Yu.N. Ponomarev, L.N. Sinitsa (Eds.), in: Proceedings of the 11th Symposium and School on High Resolution Molecular Spectroscopy, SPIE Proceedings vol. 2205, 1993, pp. 188–191.
- [27] A.G. Maki, C.C. Chou, K.M. Evenson, L.R. Zink, J.T. Shy, *J. Mol. Spectrosc.* 167 (1994) 211.
- [28] L.C. Bradley, K.L. Soohoo, C. Freed, *IEEE J. Quantum Electron.* 22 (1986) 234.
- [29] K.G. Siemsen, *Opt. Lett.* 6 (1981) 114.
- [30] D. Bailly, These, Universite de Paris-Sud, 1983.
- [31] D. Bailly, *J. Mol. Spectrosc.* 105 (1984) 215.
- [32] D. Bailly, private communication, 1997.
- [33] M.P. Esplin, H. Sakai, L.S. Rothman, G.A. Vanasse, W. Barowy, R. Huppi, AFGL-TR-0046, 1986.
- [34] S.A. Tashkun, V.I. Perevalov, J.-L. Teffo, A.D. Bykov, N.N. Lavrentieva, *J. Quant. Spectrosc. Radiat. Transfer* 82 (2003) 165.